

First measurement of the $B^+ \rightarrow \pi^+ \pi^0 \pi^0$ branching fraction and CP asymmetry

(The Belle Collaboration)

Abstract

We study $B^+ \rightarrow \pi^+ \pi^0 \pi^0$ using 711 fb^{-1} of data collected at the $\Upsilon(4S)$ resonance with the Belle detector at the KEKB asymmetric-energy e^+e^- collider. We measure the inclusive branching fraction to be $(19.0 \pm 1.5 \pm 1.4) \times 10^{-6}$ and inclusive CP asymmetry to be $(9.2 \pm 6.8 \pm 0.7)\%$, where the first uncertainties are statistical and the second are systematic; and the $B^+ \rightarrow \rho(770)^+ \pi^0$ branching fraction to be $(11.2 \pm 1.1 \pm 0.9_{-1.6}^{+0.8}) \times 10^{-6}$, where the third uncertainty is due to possible interference with $B^+ \rightarrow \rho(1450)^+ \pi^0$. We present the first observation of a structure around $1 \text{ GeV}/c^2$ in the $\pi^0 \pi^0$ mass spectrum, which has a significance of 9.2σ , and measure the branching fraction of this structure to be $(6.9 \pm 0.9 \pm 0.6) \times 10^{-6}$. We also report evidence for local CP asymmetry in this $\pi^0 \pi^0$ structure.

PACS numbers: 14.40.Nd, 13.25.Hw, 13.25.-k, 11.30.Er

Charmless three-body B decays provide a rich environment to study the properties of the weak interaction in the quark sector [1]. A study of the dynamics of such decays allows us to search for intermediate resonances and to study local CP asymmetries [2]. These are important for developing better models to describe multibody hadronic B decays. For $B \rightarrow 3\pi$, extraction of information on specific sub-decay modes is useful for constraining phases of the CKM matrix [3, 4] elements. For instance, the results for $B^+ \rightarrow (\rho\pi)^+$ and time-dependent studies of $B^0 \rightarrow (\rho\pi)^0$ [5] allow determination of the CKM angle ϕ_2 [6]. Also, interference between $B^+ \rightarrow \chi_{c0}\pi^+$ and the nonresonant decays provides useful information for extracting the angle ϕ_3 [7].

For the first measurement of the inclusive branching fraction for $B^+ \rightarrow \pi^+\pi^0\pi^0$ decays, an upper limit has been reported to be 8.9×10^{-4} at 90% confidence level (CL) [8]. The branching fraction of $B^+ \rightarrow \rho(770)^+\pi^0$ was measured by Belle [9], BaBar [10], CLEO [11], and ARGUS [8]. BaBar and LHCb also performed amplitude analyses of $B^+ \rightarrow \pi^+\pi^-\pi^+$ decays [12, 13], where intermediate resonances were investigated in detail.

In this Letter, we report measurements of the branching fraction and CP asymmetry \mathcal{A}_{CP} for $B^+ \rightarrow \pi^+\pi^0\pi^0$. We use the *sPlot* technique [14] to analyze the background-subtracted spectra, present the observation of a new structure and measure its local CP asymmetry. A major challenge in this study is the reconstruction of signal with two π^0 mesons, in which the low-momentum (soft) π^0 background has significant contribution adversely affecting our background subtraction method.

We use 772×10^6 $B\bar{B}$ pairs [15] collected at the $\Upsilon(4S)$ resonance with the Belle detector [16] at the KEKB asymmetric-energy e^+e^- collider [17].

We use Monte Carlo (MC) samples to optimize selection criteria and determine the detection efficiency. Samples of MC events for $\Upsilon(4S) \rightarrow B\bar{B}$ and hadronic continuum production $e^+e^- \rightarrow q\bar{q}$ ($q = u, d, s, c$) are generated with EVTGEN [18] and subsequently simulated with GEANT3 [20]. For signal processes, we generate a large number of MC samples for all relevant resonant decays, and nonresonant $B \rightarrow 3\pi$ decay uniformly distributed in the phase space. All resonances are modeled by relativistic Breit-Wigner distributions.

Charged particles are reconstructed with the tracking detectors [16]. Reconstructed tracks' shortest distances to the interaction point (IP) are required to be within 5.0 cm along the z axis, and within 0.3 cm in the transverse plane. The z direction is opposite the e^+ beam's direction. We use information from particle identification detectors [16, 19] to

calculate likelihood values \mathcal{L}_K and \mathcal{L}_π for kaon and pion hypotheses, respectively, for each track. Tracks with $\mathcal{L}_\pi/(\mathcal{L}_K + \mathcal{L}_\pi) > 0.6$ are identified as pions. The efficiency for identifying a pion is 90%, while the probability to misidentify kaons as pions is less than 10%.

The π^0 candidates are reconstructed from pairs of energy clusters, without associated track and reconstructed as photons, in the electromagnetic calorimeter made of CsI(Tl) crystals. To suppress beam-induced background, the reconstructed energy of each photon is required to be greater than 50 or 100 MeV if reconstructed in the barrel or end-cap regions, respectively. The invariant mass of each photon pair is required to be between 115 and 152 MeV/ c^2 , which is ± 3 units of resolution around the known π^0 mass [21]. To improve reconstruction of parent particles, the invariant masses of π^0 candidates are constrained to the known π^0 mass [21].

About 30% of events in the data sample have more than one B candidate, with an average candidate multiplicity of 1.6, primarily due to the soft π^0 background. If two or more candidates in the same event have different π^0 candidates, we select the one with the smallest sum of χ^2 values from the two π^0 mass-constrained fits; otherwise we select the candidate with the shortest transverse-plane distance between the IP and the π^+ track. In events with multiple candidates, this method selects the correct combination 92% of the time, according to simulation.

To suppress the dominant background due to hadronic continuum production, we construct a Fisher discriminant [22] from 17 modified Fox–Wolfram moments [23] and use a neural network (NN) [24] to combine the discriminant with three more variables: the cosine of the angle between the reconstructed B flight direction and the z axis in the center-of-mass (c.m.) frame, the cosine of the angle between the thrust axis [25] of the reconstructed B and that of the rest of the event in the c.m. frame, and the B meson flavor tagging quality [26]. The NN is trained with signal and continuum MC samples. Its output C_{NN} ranges from -1 to 1 and is required to be greater than 0.75 . This retains 60% of signal and removes 98% of continuum background. To simplify signal modeling, C_{NN} is transformed to $C'_{\text{NN}} \equiv \log\left(\frac{C_{\text{NN}} - C_{\text{NN}}^{\min}}{C_{\text{NN}}^{\max} - C_{\text{NN}}}\right)$, where C_{NN}^{\min} is 0.75 and C_{NN}^{\max} is the maximum value of C_{NN} , which is obtained from the MC samples.

Background events from B decays with the same final-state particles, $B^+ \rightarrow \bar{D}^0 \pi^+$ ($\bar{D}^0 \rightarrow \pi^0 \pi^0$) and $B^+ \rightarrow K_S^0 \pi^+$ ($K_S^0 \rightarrow \pi^0 \pi^0$), are removed by rejecting candidates with $M_{\pi^0 \pi^0}$ within ± 3 units of the D^0 or K_S^0 mass resolution around their nominal masses [21].

Along with the correctly reconstructed (true) signal B events in the signal MC samples, there is a sizable self-crossfeed (SCF) component arising from decay products of the other B meson, primarily due to wrong photons or π^0 's included in signal reconstruction. Soft π^0 candidates in background events give rise to a structure in phase space that complicates the $sPlot$ -based analysis since it distorts the $sWeights$ mass distributions. To alleviate this problem, we require $p_{\pi^0} > 0.5$ GeV/ c in the laboratory frame. This threshold reduces the efficiency of $B^+ \rightarrow \rho(770)^+\pi^0$ by 35%, while suppressing SCF by a factor of 2.

We obtain the total signal yield and charge asymmetry \mathcal{A}_{raw} from a three-dimensional (the beam-energy constrained mass M_{bc} , the energy difference ΔE , and C'_{NN}) extended unbinned maximum-likelihood fit to data. M_{bc} is defined as $\sqrt{E_{\text{beam}}^2/c^4 - |\vec{p}_B/c|^2}$ and ΔE is defined as $E_B - E_{\text{beam}}$, where E_{beam} is the beam energy and \vec{p}_B and E_B are the momentum and energy of the reconstructed B candidate in the c.m. frame. The signal resolution is 3 MeV/ c^2 for M_{bc} and 44 MeV for ΔE . The likelihood function is

$$\mathcal{L} = \frac{e^{-\sum_j N_j}}{N!} \prod_{i=1}^N \left(\sum_j N_j P_j^i \right), \quad (1)$$

where

$$P_j^i = \frac{1}{2} (1 - q^i \mathcal{A}_{\text{raw},j}) \times P_j(M_{\text{bc}}^i, \Delta E^i, C'_{\text{NN}}{}^i). \quad (2)$$

Here, N is the number of candidate events, fit parameter N_j is the expected number of events in category j , q^i is the charge of the π^+ in the i -th event, $\mathcal{A}_{\text{raw},j}$ is the value of the charge asymmetry of the j -th category, P_j is the 3D PDF for category j , and M_{bc}^i , ΔE^i , and $C'_{\text{NN}}{}^i$ are the values of these variables for the i -th event. The fit region is $M_{\text{bc}} > 5.26$ GeV/ c^2 , -0.3 GeV $< \Delta E < 0.15$ GeV, and $|C'_{\text{NN}}| < 8$. We model the data with four event categories: signal, continuum, B decays mediated via the dominant $b \rightarrow c$ transitions (generic B decays), and B decays mediated via $b \rightarrow u, d, s$ (rare B decays).

Owing to the shower leakage in the calorimeter [27], there is a sizable correlation between the ΔE and M_{bc} distributions for signal events. Hence, the signal PDF is a 2D smoothed histogram in ΔE -vs- M_{bc} (obtained from MC events) multiplied by the sum of two Gaussian functions and an asymmetric Gaussian function representing C'_{NN} . The signal PDF includes both true signal and SCF contributions. To correct for potential data-MC differences, signal PDF shapes are widened and shifted using a control sample of $B^- \rightarrow D^0 \rho^-$, $D^0 \rightarrow K^- \pi^+ \pi^0$ decays.

The continuum background PDF is the product of an ARGUS function [28] in M_{bc} , a first-order polynomial in ΔE , and the sum of two asymmetric Gaussian functions in C'_{NN} . Generic B decays show no peaking structure in M_{bc} and ΔE after the D^0 veto, while rare B decays, such as $B^+ \rightarrow h^+\pi^0$ and $B^0 \rightarrow \rho^+h^-$, ($h = \pi, K$), peak broadly in M_{bc} and have structure in ΔE . To account for correlations, each $B\bar{B}$ background component is modeled using a 2D smoothed histogram in ΔE -vs- M_{bc} (obtained from simulation) multiplied by the sum of two Gaussian functions representing C'_{NN} . Except for the ΔE and C'_{NN} shapes for continuum, the rest of the PDF shapes are fixed from studies of simulation. To enhance the stability of the fitter, the parameters \mathcal{A}_{raw} are fixed to zero for backgrounds, which is consistent with MC predictions.

We use the ${}_s\text{Weights}$ obtained from the 3D fit to build the signal-isolated $M_{\pi^+\pi^0}^{\text{min}}$ -vs- $M_{\pi^0\pi^0}$ histogram, where $M_{\pi^+\pi^0}^{\text{min}}$ is the smaller of the two $M_{\pi^+\pi^0}$ values for a reconstructed B candidate. In the $M_{\pi\pi}$ calculation, the momenta of the three pions are adjusted to constrain their total mass to that of the B meson. We model the decays as an incoherent sum of sub-decay modes and extract their yields from an extended weighted binned likelihood fit [29] to the 2D histogram, where the PDF of each sub-decay is a 2D smoothed histogram taken from MC simulation of this sub-decay.

The signal PDF shape, yield of the 3D fit, the ${}_s\text{Weights}$ distributions, and the 2D fit results are highly sensitive to the SCF fraction F_{SCF} . To simulate F_{SCF} correctly, we use an iterative procedure in which we generate new signal MC with a model based on the 2D-fit result. We perform the 3D fit again with a new signal PDF obtained from the new simulated sample. We perform five such iterations. The variation of F_{SCF} is less than 0.1% between the last two iterations.

From the final 3D fit, we obtain a signal yield of 1063 ± 86 events and a raw asymmetry of $\mathcal{A}_{\text{raw}} (-9.2 \pm 6.8)\%$, where the uncertainties are statistical. Figure 1(a) shows the ${}_s\text{Weights}$ $M_{\pi^+\pi^0}^{\text{min}}$ -vs- $M_{\pi^0\pi^0}$ distribution. We observe two broad clusters of events: one near the $\rho(770)^+$ resonance and another around $M_{\pi^0\pi^0} = 1 \text{ GeV}/c^2$. The latter cluster cannot be described by a single known resonance, so we model it by a sum of $f_0(500)$, $f_0(980)$, and $f_2(1270)$.

To form a baseline model, we start with a sum of nonresonant $\pi^+\pi^0\pi^0$ and $\rho(770)^+\pi^0$, then include each individual sub-decay one by one in order of mass and repeat the 2D fit. Only modes that improve the χ^2/ndf are retained; χ^2 is calculated with adaptive binning requiring the number of entries of each bin to be greater than 1.5, where ndf is the number

of degrees of freedom, the difference between the number of bins (127) and the number of PDF's in the 2D fit. The baseline model contains nonresonant $\pi^+\pi^0\pi^0$ decay, $\rho(770)^+\pi^0$, $f_0(500)\pi^+$, $f_0(980)\pi^+$, $f_2(1270)\pi^+$, and $\rho(1450)^+\pi^0$. Including each of $B^+ \rightarrow f_0(1370)\pi^+$, $\chi_{c0}\pi^+$, or $\chi_{c2}\pi^+$ modes does not improve the fit and predicts a yield consistent with zero. Figures 1(b) and (c) show $M_{\pi^+\pi^0}^{\min}$ and $M_{\pi^0\pi^0}$ projections of the data and fit results with the baseline model. The model describes the data well with a χ^2/ndf of 0.93.

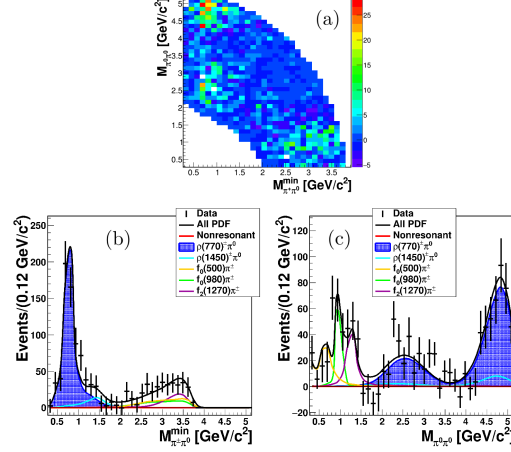


FIG. 1: $sWeights$ $M_{\pi^+\pi^0}^{\min}$ -vs- $M_{\pi^0\pi^0}$ distribution, its projections, and the results of the 2D fit.

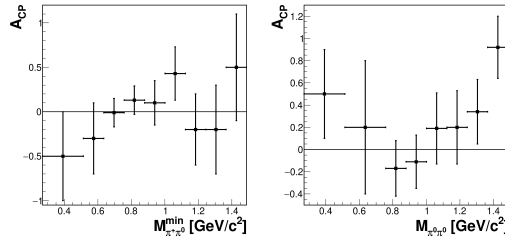


FIG. 2: $sWeights$ \mathcal{A}_{CP} vs $M_{\pi^+\pi^0}^{\min}$ for $M_{\pi^0\pi^0} > 1.9 \text{ GeV}/c^2$, and vs $M_{\pi^0\pi^0}$ for $M_{\pi^+\pi^0}^{\min} > 1.9 \text{ GeV}/c^2$.

The first few bins are combined due to small statistics.

The branching fractions of $B^+ \rightarrow \pi^+\pi^0\pi^0$ and its sub-decays are

$$\mathcal{B} = \frac{N_{\text{sig}}}{\epsilon \times N_{B\bar{B}}}, \quad (3)$$

where N_{sig} and ϵ are the signal yield and reconstruction efficiency for each decay, and $N_{B\bar{B}}$ is the number of $B\bar{B}$ events. Both true and SCF events are regarded as signal in this formula. We assume equal branching fractions for the $\Upsilon(4S)$ decaying into charged and neutral $B\bar{B}$

pairs. The efficiency for the inclusive decays is calculated using an MC sample of the final baseline model. F_{SCF} is 20.7% for the inclusive decays and ranges from 10% to 25% for sub-decay modes.

A summary of our results is shown in Table I. We do not report branching fractions for $f_0(500)\pi^+$, $f_0(980)\pi^+$, and $f_2(1270)\pi^+$ due to the significant overlap and insufficient interference information. As the region $M_{\pi^0\pi^0} < 1.9 \text{ GeV}/c^2$ and $M_{\pi^+\pi^0}^{\text{min}} > 1.9 \text{ GeV}/c^2$ contains little contribution from nonresonant decay and ρ modes, we calculate the branching fraction of $X\pi^+$, where X stands for the total resonant $\pi^0\pi^0$ contribution, using the yield, 366_{-48}^{+50} , of the 3D fit within that region. The statistical significance of this yield is 9.2σ , defined as $\sqrt{2\ln(\mathcal{L}/\mathcal{L}_0)}$, where \mathcal{L} and \mathcal{L}_0 are the maximum likelihoods of the fits with and without the signal component.

Upper limits at 90% CL are reported for the modes with signals of statistical significance less than 3σ using the frequentist method. For each, we generate large toy MC ensembles based on the result in Table I and fit to these to obtain the yield distribution. From this we calculate the upper limit at 90% CL. Systematic uncertainties are included by applying Gaussian smearing to the yield distributions. Possible interferences between resonances are not included in this procedure. The asymmetry in π^+ detection is estimated using a control sample of $D^+ \rightarrow K_S^0\pi^+$ [30] as -0.03% , and is subtracted from \mathcal{A}_{raw} to calculate \mathcal{A}_{CP} .

The local CP asymmetries obtained from the $sWeights$ histograms of B^+ and B^- are shown in Fig. 2. The regions above $1.49 \text{ GeV}/c^2$ are not shown as the $sWeights$ values are consistent with 0. \mathcal{A}_{CP} is consistent with 0 everywhere except for the $M_{\pi^0\pi^0}$ region between $1.36 \text{ GeV}/c^2$ and $1.49 \text{ GeV}/c^2$, which has $\mathcal{A}_{CP} = (92 \pm 28)\%$. By performing an additional 3D fit to this region with \mathcal{A}_{CP} floated in the range $[-1,1]$ and \mathcal{A}_{CP} fixed to zero, we calculate a statistical significance of 3.2σ for nonzero \mathcal{A}_{CP} .

Various sources of systematic uncertainties are considered for all branching fractions. To obtain the overall value for each decay mode, all relevant independent uncertainties are summed quadratically. The reconstruction efficiency is calibrated for data-MC discrepancies using dedicated control samples; the small corrections are applied and their uncertainties are taken as systematic uncertainties. An uncertainty due to the number of $B\bar{B}$ events is 1.4%. An uncertainty due to charged-track reconstruction is estimated to be 0.35% per track from $D^{*+} \rightarrow D^0\pi^+$ with $D^0 \rightarrow \pi^+\pi^-K_S^0$. An uncertainty due to π^+ identification is estimated to be 0.9% from $D^{*+} \rightarrow D^0\pi^+$ with $D^0 \rightarrow K^-\pi^+$. An uncertainty due to

TABLE I: Summary of the results. The masses and widths (in MeV/ c^2) used in the 2D fit, signal selection efficiencies, fitted yields, branching fractions, and \mathcal{A}_{CP} are shown. The values in parentheses are the upper limits of branching fraction at 90 CL. The first error is statistical and the second is systematic. The interference effect is included in the analysis of the $\rho(770)^+\pi^0$ mode as the third uncertainty.

Decay mode	Mass	Width	ϵ (%)	Fitted yield	\mathcal{B} (10^{-6})	\mathcal{A}_{CP} (%)
$\pi^+\pi^0\pi^0$ (inclusive)			7.2	1063 ± 86	$19.0 \pm 1.5 \pm 1.4$	$9.2 \pm 6.8 \pm 0.7$
Non-resonant			10.6	3 ± 14	$0.03 \pm 0.16^{+0.12}_{-0.15}$ (< 0.6)	–
$\rho(770)^+\pi^0, \rho(770)^+ \rightarrow \pi^+\pi^0$	775.5	150.3	7.3	637 ± 65	$11.2 \pm 1.1 \pm 0.9^{+0.8}_{-1.6}$	$8.0 \pm 15.0^{+2.3}_{-7.5}$
$\rho(1450)^+\pi^0, \rho(1450)^+ \rightarrow \pi^+\pi^0$	1465	400	8.6	80 ± 51	$1.2 \pm 0.6 \pm 0.2$ (< 2.5)	–
$f_0(500)\pi^+, f_0(500) \rightarrow \pi^0\pi^0$	600	400	7.1	123 ± 37	–	–
$f_0(980)\pi^+, f_0(980) \rightarrow \pi^0\pi^0$	980	50	8.7	102 ± 30	–	–
$f_2(1270)\pi^+, f_2(1270) \rightarrow \pi^0\pi^0$	1275.4	185.1	5.6	119 ± 32	–	–
$X\pi^+, X \rightarrow \pi^0\pi^0$	–	–	6.9	366^{+50}_{-48}	$6.9 \pm 0.9 \pm 0.6$	$18.2 \pm 11.6 \pm 0.7$
$f_0(1370)\pi^+, f_0(1370)^0 \rightarrow \pi^0\pi^0$	1400	300	9.0	< 75	< 1.1	–
$\chi_{c0}\pi^+, \chi_{c0} \rightarrow \pi^0\pi^0$	3415.2	10.2	11.1	< 39	< 0.5	–
$\chi_{c2}\pi^+, \chi_{c2} \rightarrow \pi^0\pi^0$	3556.3	2.0	11.5	< 63	< 0.7	–

π^0 reconstruction is estimated to be 4.8% from $\tau \rightarrow \pi^-\pi^0\nu_\tau$ [31]. An uncertainty due to continuum suppression based on C_{NN} is estimated to be 1.4% from $B^- \rightarrow D^0\rho^-$ with $D^0 \rightarrow K^-\pi^+\pi^0$. The uncertainty in estimating the reconstruction efficiency due to the MC statistics is 0.02%.

To estimate the systematic uncertainty associated with fixed PDF shapes in the 3D fit, we vary the shapes of signal PDF and PDFs represented by analytical functions according to their respective uncertainties, and vary the binning schemes of all the other smoothed histograms. The resulting changes in the signal yield are added in quadrature. To account for possible data-MC difference on F_{SCF} in the signal PDF, we vary it within $\pm 30\%$ of nominal. The total systematic uncertainty is 5.5%.

Possible variation of the signal model composition is estimated from the iteration pro-

cedure. We take the difference between yields in the last two iterations as a systematic uncertainty, 0.7%. Possible bias due to the *sPlot* technique is estimated to be 2.9% from the difference between the 3D fit yield and the sum of *sWeights* in the limited Dalitz region.

While validating the entire fit procedure using large sample of pseudo-experiments, small biases are identified in both 3D and 2D fits. They result in $(0.04\text{--}0.18)\times 10^{-6}$ changes in branching fractions and are included as systematic uncertainties. The uncertainty due to each resonance's parameters is estimated. The mass and width are varied by ± 1 unit of their uncertainties, or over their entire range [21]; all changes in the yield are added in quadrature and taken as a systematic uncertainty. For the nonresonant decay PDF, the effect of varying its template's binning is studied. Since the nonresonant decay and $\rho(1450)^+\pi^0$ are the two least significant components in the 2D fit, we also consider the nonresonant decay's yield discrepancy with and without $\rho(1450)^+\pi^0$ PDF. The uncertainty range is between 0.003×10^{-6} and 0.42×10^{-6} .

A systematic uncertainty in the efficiency for the inclusive decay due to decay-model uncertainties is estimated to be 1.6% from the difference between the nominal measurement of the branching fraction and its value obtained by summing over an efficiency-corrected *sWeights* yields for all bins of $M_{\pi^+\pi^0}^{\min}$. The uncertainty due to the $X \rightarrow \pi^0\pi^0$ model composition is estimated to be 2.9% from the change in the efficiency when varying the fitted yields of $f_0(500)\pi^+$, $f_0(980)\pi^+$, and $f_2(1270)\pi^+$ by ± 1 unit of their uncertainties.

The uncertainty in the $B \rightarrow X\pi^+$ branching fraction due to nonresonant and ρ contamination is estimated to be 3.3% from the difference between the 3D fit yield and the sum of the 2D fit yields of the three resonances.

To estimate the systematic uncertainty due to interference between $\rho(770)^+$ and $\rho(1450)^+$, large toy MC ensembles with different phase differences and amplitude ratios are generated. We fit to them using the incoherent sum of the PDFs for the two ρ 's and take the largest deviation between the fitted and the input amplitude ratios as a systematic uncertainty.

Several sources of systematic uncertainty on \mathcal{A}_{CP} are considered. The uncertainty due to π^+ detection asymmetry is estimated to be 0.3% using a control sample of $D^+ \rightarrow K_S^0\pi^+$ [30]. An uncertainty due to fixing the PDF shapes in the 3D fit for the overall \mathcal{A}_{CP} is studied using methods similar to that used for the branching fraction and is estimated to be 0.5% by varying the PDF shapes. Similarly, the uncertainty due to resonance shape parameters in the 2D fit is estimated to be ${}_{-7.5}^{+2.2}\%$ for $\rho(770)^+\pi^0$ by varying resonance shape parameters.

The uncertainty due to the fixed background \mathcal{A}_{CP} in the 3D fit is estimated to be 0.5% from the change in the results when these are floated. A systematic effect on \mathcal{A}_{CP} due to interference between $\rho(770)^+\pi^0$ and $\rho(1450)^+\pi^0$ is negligible as determined from a study similar to that for the branching fraction.

In conclusion, we have performed a study of $B^+ \rightarrow \pi^+\pi^0\pi^0$ using 711 fb^{-1} of data collected by Belle. We measure the inclusive branching fraction $\mathcal{B}(B^+ \rightarrow \pi^+\pi^0\pi^0) = (19.0 \pm 1.5 \pm 1.4) \times 10^{-6}$ and CP asymmetry $\mathcal{A}_{CP} = (9.2 \pm 6.8 \pm 0.7)\%$, where the first uncertainties are statistical and the second are systematic. We report the composition of intermediate states in $B^+ \rightarrow \pi^+\pi^0\pi^0$ within our model and measure the local CP asymmetry. The branching fraction of $B^+ \rightarrow \rho(770)^+\pi^0$ is measured to be $(11.2 \pm 1.1 \pm 0.9_{-1.6}^{+0.8}) \times 10^{-6}$, where the third uncertainty accounts for possible interference with $B^+ \rightarrow \rho(1450)^+\pi^0$. We observe a structure, likely arising due to multiple resonances, at $M_{\pi^0\pi^0} < 1.9 \text{ GeV}/c^2$ and $M_{\pi^+\pi^0}^{\min} > 1.9 \text{ GeV}/c^2$ with an inclusive branching fraction of $(6.9 \pm 0.9 \pm 0.6) \times 10^{-6}$. We find evidence for non-zero local CP asymmetry at $1.36 \text{ GeV}/c^2 < M_{\pi^0\pi^0} < 1.49 \text{ GeV}/c^2$ and $M_{\pi^+\pi^0}^{\min} > 1.9 \text{ GeV}/c^2$, which is similar to the asymmetry in $B^+ \rightarrow f_2(1270)\pi^+$ observed for $B^+ \rightarrow \pi^+\pi^-\pi^+$ [12, 13]. We do not observe $B^+ \rightarrow f_0(1370)\pi^+$, $B^+ \rightarrow \chi_{c0}\pi^+$, or $B^+ \rightarrow \chi_{c2}\pi^+$. An amplitude analysis with improved treatment of systematic effects from π^0 reconstruction is needed to further understand the properties of the $B^+ \rightarrow \pi^+\pi^0\pi^0$ transition. Eventually, the larger data set and better performance for neutral particle reconstruction at Belle II [32, 33] will make it possible to carry out such an analysis.

We thank the KEKB group for the excellent operation of the accelerator; the KEK cryogenics group for the efficient operation of the solenoid.

-
- [1] E. Kou *et al.*, Prog. Theor. Exp. Phys. **2019**, 123C01 (2019) Section 12.7 [Erratum: Prog. Theor. Exp. Phys. **2020**, 029201 (2020)].
 - [2] I. Bediaga *et al.*, Phys. Rev. D **86**, 036005 (2012).
 - [3] N. Cabibbo, Phys. Rev. Lett. **10**, 531 (1963).
 - [4] M. Kobayashi and T. Maskawa, Prog. Theor. Phys. **49**, 652 (1973).
 - [5] Throughout this paper, inclusion of charge-conjugate decay modes is implied.
 - [6] A. E. Snyder and H. R. Quinn, Phys. Rev. D **48**, 2139 (1993).

- [7] B. Bajc *et al.*, Phys. Lett. B **447**, 313–320 (1999).
- [8] H. Albrecht *et al.* (ARGUS Collaboration), Phys. Lett. B **241**, 278 (1990).
- [9] J. Zhang *et al.* (Belle Collaboration), Phys. Rev. Lett. **94**, 031801 (2005).
- [10] B. Aubert *et al.* (BaBar Collaboration), Phys. Rev. D **75**, 091103 (2007).
- [11] C. P. Jessop *et al.* (CLEO Collaboration), Phys. Rev. Lett. **85**, 2881 (2000).
- [12] B. Aubert *et al.* (BaBar Collaboration), Phys. Rev. D **79**, 072006 (2009).
- [13] R. Aaij *et al.* (LHCb Collaboration), Phys. Rev. D **101**, 012006 (2020).
- [14] M. Pivk and F. R. Le Diberder, Nucl. Instrum. Methods Phys. Res., Sect. A **555**, 356 (2005).
- [15] J. Brodzicka *et al.*, Prog. Theor. Exp. Phys. **2012**, 04D001 (2012) Section 2.
- [16] A. Abashian *et al.* (Belle Collaboration), Nucl. Instrum. Methods Phys. Res., Sect. A **479**, 117 (2002).
- [17] S. Kurokawa and E. Kikutani, Nucl. Instrum. Methods Phys. Res., Sect. A **499**, 1 (2003), and other papers included in this volume; T.Abe *et al.*, Prog. Theor. Exp. Phys. **2013**, 03A001 (2013) and references therein.
- [18] D. J. Lange, Nucl. Instrum. Methods Phys. Res., Sect. A **462**, 152 (2001).
- [19] E. Nakano, Nucl. Instrum. Methods Phys. Res. Sect. A **494**, 402 (2002).
- [20] R. Brun *et al.*, GEANT 3.21, CERN Report No. DD/EE/84-1, 1987.
- [21] P. A. Zyla *et al.* (Particle Data Group), Prog. Theor. Exp. Phys. **2020**, 083C01 (2020).
- [22] R. A. Fisher, Ann. Human Genet. **7**, 179 (1936).
- [23] G. C. Fox and S. Wolfram, Phys. Rev. Lett. **41**, 1581 (1978). The modified moments used in this paper are described in S. H. Lee *et al.* (Belle Collaboration), Phys. Rev. Lett. **91**, 261801 (2003).
- [24] M. Feindt and U. Kerzel, Nucl. Instrum. Methods Phys. Res., Sect. A **559**, 190 (2006).
- [25] S. Brandt, C. Peyrou, R. Sosnowski, and A. Wroblewski, Phys. Lett. **12**, 57 (1964).
- [26] H. Kakuno *et al.*, Nucl. Instrum. Methods Phys. Res., Sect. A **553**, 516 (2004).
- [27] K. Miyabayashi, Nucl. Instrum. Methods Phys. Res., Sect. A **494**, 298 (2002).
- [28] H. Albrecht *et al.* (ARGUS Collaboration), Phys. Lett. B **241**, 278 (1990).
- [29] W. Verkerke and D. P. Kirkby, eConf **C0303241**, MOLT007 (2003) [arXiv:physics/0306116 [physics]].
- [30] B. R. Ko *et al.* (Belle Collaboration), Phys. Rev. Lett. **109**, 021601 (2012).
- [31] S. Ryu *et al.* (Belle Collaboration), Phys. Rev. D **89**, 072009 (2014).

- [32] T. Abe *et al.* (Belle II Collaboration), arXiv:1011.0352 [physics.ins-det], (2010).
- [33] E. Kou *et al.*, Prog. Theor. Exp. Phys. **2019**, 123C01 (2019) Section 5.6 [Erratum: Prog. Theor. Exp. Phys. **2020**, 029201 (2020)].